Wear, Volume 256, Issues 9-10, May 2004, Pages 907-917.

High Temperature Erosion-Oxidation Mechanisms, Maps and Models

R.G Wellman and J.R Nicholls

School of Industrial and Manufacturing Science

Cranfield University, Bedford,

MK 43 OAL, UK.

Abstract

The aim of this paper is to provide an overview of erosion-oxidation studies by reviewing the work that has been done on mechanisms, maps and models. High temperature erosion-oxidation is a major cause of wear in both fluidised bed combustors and gas turbines and much effort has been put into understanding the phenomena and reducing wear rates. A number of different erosion-oxidation mechanisms have been proposed over the years to describe the different wear regimes, some of these mechanisms are discussed in this paper, as well as the mapping techniques that have been used to quantify wastage rates. Finally, erosion-oxidation modelling is discussed, starting with models that combine oxidation kinetics with erosion rate equations that lead to predictive models before concentrating on Monte Carlo modelling methods.

1. Introduction

Erosion affects numerous industries, such as power generation, mining and the pneumatic transportation of solids, while the marine, oil and gas, chemical and power generation industries are all primarily affected by corrosion and oxidation and to a lesser extent erosion. But the worst case scenarios normally occur where there is a combination of both erosion and corrosion or oxidation especially in the cases of erosion and high temperature oxidation as in gas turbine engines and fluidised bed combustors (FBCs). There are occasions when oxidation can reduce the degree of materials loss by such wear processes by forming a stable

protective oxide layer, often referred to as an oxide glaze, but more often than not the combination results in excessively high wear rates. In order to understand the interactions between the two processes it is necessary to have an understanding of both processes on their own before trying to predict how they behave in combination.

This paper gives a succinct overview of erosion mechanisms and oxidation kinetics before discussing erosion-oxidation (E-O) mechanisms, maps and models. The two main industries that triggered the research into E-O are FBCs and gas turbines, both of which operate at opposite ends of the E-O spectrum. FBCs operate under high particle fluxes and low velocities 1-10m/s while gas turbine engines operate at low particle fluxes but high impact velocities (in the region of 300m/s).

2. Basic Erosion Mechanisms

Erosion mechanisms can be broadly divided into two main categories: ductile erosion and brittle erosion. The major difference between the two erosion mechanisms becomes obvious when comparing the erosion rate at different angles of impact. In the erosion of ductile materials the maximum erosion rate is usually found to occur at an impact angle of between 30 and 60 degrees, while in brittle materials this will occur at approximately 90° impact.

2.1 Impact damage in ductile materials

The erosion of soft, tough materials is predominantly ductile and material loss can occur in two different ways: cutting wear due to impact at low angles [1], and extrusion at high angles. Fragmentation of the impacting particles can occur at normal or near-normal impact angles, giving rise to secondary erosion [2]. These two mechanisms are not mutually exclusive, and

erosion of ductile materials is essentially a combination of the two processes, with one being dominant over the other depending on impact angle and material properties and particle properties and shape.

2.2 Cutting wear

Ductile erosion reaches a maximum at a particular angle for a given system, usually between 30 and 60°, due to cutting wear. The impacting particle removes material by chip formation, essentially scraping material off the surface of the solid in a manner similar to machining [1].

2.3 Extrusion and Fragmentation

When the eroding particle strikes the surface of a ductile material at or near 90° the material is extruded to the edge of the damage zone to form lips that will then be vulnerable to subsequent impacts [2][3]. These subsequent impacts will cause further deformation, extrusion and work hardening, until fracture occurs and the material is completely lost from the surface. A secondary stage can also occur when the impacting particles are brittle and fracture on impact, resulting in further secondary impact damage at a reduced velocity and lower impact angles. There are many papers available in the literature which deal with calculating and modelling the wear rates of ductile materials[1,3-5].

2.4 Impact damage in brittle materials

Material loss in solid particle erosion of brittle materials occurs predominantly through the formation and interaction of a subsurface microcrack network. In order for these cracks to develop, the surface stresses must reach a critical value to initiate microcracking. When these

cracks propagate and intersect with the surface, material is lost [1,6-9]. Hence for a brittle material the erosion resistance is a function of its fracture toughness and its resistance to crack initiation.

The modes of deformation and fracture depend on the particle velocity, shape, and its mechanical properties relative to those of the target material [1,10-12]. Blunt particles travelling at low velocities set up hertzian stress fields in the target, which initiate cone cracking, while angular particles travelling at high velocities produce inelastic deformation zones and initiate median and lateral cracking [13].

2.5 Median / Lateral cracking

When eroding brittle materials with relatively hard or incompressible particles the target is plastically deformed and two primary types of fracture can occur. Median cracks propagate downward from the contact zone, and lateral cracks develop below the contact zone and propagate parallel to the surface, eventually curving up towards the surface [6]. These cracks exhibit some similarities to the median and lateral cracks observed during quasi-static indentation [14].

Lawn and Swain [14] have described the loading sequence for a sharp indenter in the following way. An initial zone of irreversible deformation, which increases with increasing load, is induced around the sharp indenter. Once a critical load has been reached, a crack will initiate under the contact point where the stress concentration is greatest. This crack is called the median vent and on initial unloading it will begin to close but does not heal. Relaxation of the deformed material within the contact zone, just prior to removal of the indenter,

superimposes intense residual tensile stresses upon the applied field. This in turn causes the

initiation of sideways extending cracks called lateral cracks. On complete unloading the lateral crack continues to grow and can intersect the surface, causing material loss [14-17]. Material loss occurs due to intersection of lateral cracks with the surface as well as interaction with other cracks.

2.6 Hertzian cracking

When a blunt elastic particle impacts on a brittle material, which remains elastic until fracture occurs, Hertzian cone cracks will develop. Material removal will depend on the propagation of the fracture into the material and its interaction with other fractures.

On initial loading, a compressive field is set up directly beneath the indenter, with a tensile stress outside the expanding contact circle. As the tensile stress increases the stage is reached where an inherent surface flaw in the material is subjected to sufficient tensile stress to initiate crack propagation. This crack will then propagate around the area of contact to form a ring crack, which will extend downwards out of the surface region. As loading increases, tensile stresses develop until the ring crack spontaneously develops into a full cone crack. On unloading, the cone crack will attempt to close and heal in order to recover some of the stored elastic energy but is prevented from doing so by the mechanical obstruction of debris. If the unloading is rapid enough, the base of the cone may turn up in a hat brim fashion and could intersect the surface [1,18].

3. Erosion-Oxidation

The big question is what happens when both erosion and oxidation are combined. It all depends on the oxidation kinetics of the system being investigated, i.e. fast growth (e.g. NiO) or slow growth (e.g. Cr_2O_3) oxide, temperature, whether the oxide is protective, its mechanical

properties and the erosion conditions. First consider the fundamentals of oxide growth.

3.1 Oxidation and Oxide Growth from an Erosion Perspective

Oxidation is a thermochemical process. That is all metals, when exposed at high temperature, move towards a thermodynamic equilibrium with their environment. This manifests itself, for most structural materials, in the growth of a surface oxide scale. In alloy systems there is competition between the various alloy constituents which gives rise to selective oxidation, the formation of multilayered scales, internal oxidation and other more complex bioxidant oxidation reactions.

With such a thermodynamic background in mind, for alloy systems, one initially observes the formation of a ‘transient oxide’ on an exposed metallic alloy surface. The transient oxide usually contains stable oxide species of all the oxidisable elements in the alloy. Competition between the growth of these species usually leads to the formation of some protective oxide, be it alumina, chromia or an iron-chromium spinel, depending on the alloy being oxidised. This is the desirable service condition, with components protected by a stable, slow growing surface oxide. The kinetics of this has been well researched for many alloy systems, with protective oxide growth following parabolic or sub-parabolic kinetics. Problems are
encountered when this oxide scale is damaged, be it due to ballistic impaction, erosion, mechanical stressing, or thermal cycling, when non protective oxidation may ensue leading to thicker oxide scales and faster oxidation rates.

The onset and extent of such mechanically induced failures depends primarily on interplay between three factors:

i) defects, such as voids, pores and microcracks that develop in the scale as it grows [19-23].

ii)stresses that act on the scale. These may result from impact events, but are supplemented by those generated due to oxide growth and due to thermally induced transients within the system under evaluation. The influences of such stresses will be locally concentrated by the defects in the scale.

iii) stress relief within the oxide scale/substrate system can limit the extent of such mechanical failures of the oxide scale. This occurs primarily by plastic deformation of the near surface region, while at temperature . From an erosion-oxidation perspective this stress relief has a significant influence on the boundary between 'oxide modified' and 'substrate dominated' erosion, using the terminology of Stephenson and Nicholls [24].

The interaction between these three factors, and how they depend on the impact event, will determine when scale failure occurs. The mechanically damaged scale can be healed by forming a new oxide - this involves both the transient oxidation and protective growth stages – and the relative times between this oxide loss, healing and re-growth process dictates the observed erosion-oxidation regime.

One final point, continued impact, scale spallation and re-growth, will lead to depletion of oxide forming elements from within the near surface region of the alloy. This will have an influence on the type of oxide formed, its mechanical properties and the mechanical properties of the underlying alloy. These time dependent phenomena further complicate the modelling/prediction of erosion-oxidation. For example FeCrAlY steels produce an adherent alumina scale when the Al content in the near surface region is above 2wt%, below this it forms chromia scales and finally base metal oxides these scales are less adherent and less protective than alumina.

3.2 Erosion-Oxidation Mechanisms

Over the years, particularly in the 80's and early 90's, there has been a lot of research conducted on high temperature erosion [25-43], with most of the work concentrating on stainless steels, nickel based superalloys and titanium alloys, although some work was also conducted on ceramics.

There have been a number of different approaches used to deal with and quantify the erosion oxidation problem. These include lab testing of various types - a review of which has been published by Nicholls [44] - in situ testing [45,46] and various modelling [24,47-50] and mapping techniques [51,52], which will all be discussed in the following sections.

There are a number of factors that have been found to influence the E-O of materials which include, particle size, velocity, density, angularity and hardness, the time between impacts (particle flux) as well as the angle of impact and of course the oxidation kinetics, which is affected by the temperature and the alloy composition. Hogmark [53] stated that in order to characterise the E-O of a material one needed to know the following:

- The oxidation properties of the base metal.
- The erosion properties of the base metal.
- The erosion properties of the oxide layer.
- The erosion properties of the base metal coated with an oxide layer.

The oxidation properties of the base metal combined with the flux of the erodent will determine the thickness of the oxide that is formed; the velocity and size of the particles will also have an influence. Thus Barkalow and Pettit[54] defined E-O in terms of the kinetic energy of the impacting particles and scale growth rate identifying various regimes as illustrated in Figure 1.

The erosion properties of the oxide layer become important when the impact energy and the particle flux are both sufficiently low that the oxide grows to a sufficient thickness that the impact event is totally contained within the oxide layer and is not affected by the substrate. The erosion properties of the base layer coated with an oxide layer become important when the oxide layer is not thick enough to contain the whole impact event and the substrate as well as the oxide is deformed. The combination of these different factors led to the need to define different erosion regimes/mechanisms relating to particle size, flux and velocity and oxide/substrate interactions.

Most researchers have divided the erosion-oxidation process into four or six different regimes ranging from pure erosion on one side to pure oxidation on the other with various intermediate regimes. Some of the proposed regimes are summarised in table 1.

Laboratory testing seemed to indicate that there was a distinct erosion-corrosion response to temperature, with wastage rates increasing with an increase in temperature to some peak temperature before starting to decrease with a further increase in temperature [29] as illustrated in Figure 2 [40]. This was different to the findings from in situ testing in FBC's where E-O wastage was found to decrease with an increase temperature after a critical temperature was passed, as illustrated in Figure 3. This 'anomaly' was attributed to the fact that in laboratory testing the specimens where not internally cooled, as is the case for heat exchanger tubes.

These findings prompted the modifications to the erosion-corrosion test rig at Cambridge to enable it to test internally cooled specimens [28], which would be more representative of the actual conditions with in a fluidized bed combustor. It was found that specimens tested under isothermal conditions showed a maximum wastage rate at intermediate temperatures (about 3 50°C), while those tested with internal cooling exhibited maximum wastage rates in the region of 200°C, which is similar to that experienced in FBCs as illustrated in Figure 3. It was

proposed that internal cooling of the specimens caused the isothermal erosion-corrosion curve to broaden, shifting the maximum wastage rates to lower temperatures.

Over the years different E-O regimes have been observed under various conditions by different researches, Sethi et al [29] described the E-O regions as low- intermediate- and high-temperature regimes, similar to Stack's erosion dominated, erosion-corrosion dominated and corrosion dominated regimes [40]. Stephenson and Nicholls [24] termed these regimes substrate dominated, oxide modified and oxide dominated erosion in their work on various alloys.
Essentially most of the proposed mechanisms are similar, if not identical and will now be discussed in more detail. In the first of these regimes where the oxide scale is very thin the erosion rate is relatively insensitive to increases in temperature and depends mainly on the properties of the base metal - substrate dominated erosion. However, as the temperature increases the second regime is entered and the erosion rate increases due to the formation and easy removal of the oxide scale - oxide modified erosion. Here the erosion rate is dependent on the properties of the composite oxide/substrate, the ease with which the scale is removed and the oxidation kinetics. The third regime is where the oxide forms sufficiently quickly and is thick enough that the impact of particles does not expose the base metal. Thus only oxide is removed during impacts - oxide dominated erosion. The temperatures at which these various regimes operate depend on a number of factors, which include particle size, velocity and flux as well as the composition of the alloy, which influences oxidation rates.

Rishel's description is very similar to that of Stephenson's but includes three different erosion enhanced corrosion regimes, illustrated in Figure 5. Type III, which is the same as the oxide modified regime proposed by Stephenson, involving spallation of the oxide. In type I and type II the thickness of the oxide is reduced due to erosion and hence the rate of oxidation increases compared to pure oxidation also cracks caused by the impacting particles facilitate the diffusion

of oxygen to the metal surface further increasing the oxidation rate.

There are a few other factors affecting E-O that need to be mentioned here, namely alloy content and oxide morphology. If the oxide forms a segmented scale the E-O wastage rate per impact is limited by the crystallite size. However, if a thick continuous oxide is formed each impact will be able to remove more material resulting in a higher wastage rate [61]. It has been shown that Si additions to low Cr steels reduces the E-O wastage rate due to the formation of a segmented oxide scale [62] as opposed to a continuous oxide scale.

As can be seen from Figure 6 the alloy content can shift the E-O trend depending on whether the material becomes more or less corrosion resistant. However, these effects are not always observed and this “typical response” is dependent on whether the oxide formed is coherent and adherent and the point at which it will spall. In the case of non-protective oxides erosion-corrosion rates will increase dramatically as the temperature increases, since the third regime can not be attained. Levy [61] showed that increasing the Cr content (in Cr containing alloys) reduced the E-O wastage rate and that at the conditions used (850°C, 35 m/s, 130 µm Al_2O_3) the mechanism changed from oxidation controlled erosion to oxidation affected erosion in the region of 15% Cr.

3.3 Erosion-Oxidation Mapping

Erosion-oxidation mapping (E-O maps) and more recently erosion-corrosion (aqueous) mapping (E-C maps) have become a popular way in which to represent the way in which a system will behave under different E-O and E-C conditions. E-O maps can be plotted in a number of different ways. Stephenson and Nicholls [24] plotted particle velocity vs oxide thickness for a specific particle size and temperature, while Stack [38] plotted velocity vs

temperature. In both cases contours indicate the different regimes of E-O wastage, which translate into regions of high, medium and low mass loss as shown in the following figures. As the following diagrams indicate, E-O maps are useful to determine what will happen when conditions change, ie if flux or velocity increase or if there is a change in oxidation kinetics due to a change in alloy, the different mechanisms operating and the rough position of boundaries between each of the mechanisms.

As can be seen in Figure 7 and Figure 8 as the velocity increase so does the temperature associated with the change in the E-O regime. While from Figure 8 (when compared to Figure 7) an increase in oxidation rate decreases the temperature at which regimes change for a set velocity. Stack also showed that by increasing the flux (ie reducing the time between impacts), which effectively reduces the oxide thickness, the transition boundaries move to higher temperatures.

Stephenson and Nicholls took the concept of maps one step further by adding wastage rate contours to E-O maps of impact velocity vs particle size for a set temperature. The wastage rates were calculated by an E-O Monte Carlo model, which was capable of differentiating between the different E-O regimes for each impact event.

The major draw back with E-O maps is that in order to fully characterise a system one needs a whole family of maps to cover the main variables namely, velocity temperature and particle size and flux. This has recently been done by Stack and Pena [51] who produced a family of wear maps of velocity vs particle size for three different compositions and four different temperatures. The maps were produced from a family of graphs of thickness loss vs velocity for three different particle sizes and four different temperatures for four different compositions. These were then used to produce materials performance maps from the low wastage regimes of

the E-O maps.

3.4 Erosion-Oxidation Modelling

From the modelling side there are two main routes that have been followed. The first involves an ‘equation’ approach where the oxidation kinetics of a system are combined with simple mass (or volume) loss equations to generate a single complex equation to predict mass loss due to E-O, such as those produced by Markworth [49] and Stack [50]. This type of model has a limited accuracy and is normally only valid for one of the E-O mechanisms discussed earlier and are possibly alloy specific.

The model proposed by Markworth et al [49] was based on their observation on the erosion-oxidation of AISI 446 SS and Stellite 6B and made two major assumptions:

- That the alloy would always be covered with an oxide layer.
- That in an erosion event, the erodent would only remove the oxide layer and not the substrate alloy.

These two assumptions meant that the model was effectively limited in accuracy and was only valid under the oxide modified regime discussed earlier. The model was based on parabolic oxidation kinetics and that the erosion rate was proportional to scale thickness leading to a single mass loss equation.

The model was subsequently expanded [48] by defining an erodent contact footprint, and hence a volume of oxide removed (all the oxide under the footprint was removed). Footprint size was based on experimental observations and again a single mass loss equation was derived. This model thus assumes that all impact events are the same and that there is no

influence of particle size variations on the results and it does not take into account the effect of

impact angle.

Stack's [50] model divided E-O into four regimes and was based on the assumption that there was a parabolic oxidation rate between impacts and that the oxidation that occurred during impact was negligible. It was also assumed that the critical scale thickness marked the limiting thickness which could be removed above the critical temperature. By defining weight gain per unit area as a function of time and temperature and mass loss due to erosion as a function of time per unit area Stack et al were able to construct E-O maps of velocity vs temperature and to determine how various factors changed the transition zones on the E-O maps as shown in figures 7 and 8.

Another, rather more complex, approach, which was taken by Stephenson and Nicholls [63,64], was to use a Monte Carlo statistical approach, where the damage caused by each individual impacting particle is quantified. Although more complex, this enables the model to assess each particle/oxide (or substrate) interaction and ascertain the E-O regime and determine the amount of material removed as a result of the local impact conditions. Recently, a similar approach has been used to model the erosion of electron beam physical vapour deposited thermal barrier coatings [65,66].

In order to model E-O using Monte Carlo methods the following parameters need to be known and quantified:

These parameters are known to be significant factors in the erosion-oxidation process and should also, ideally, be considered when developing analytical solutions.

Consider now, the erosion of an oxide covered metallic surface, as discussed above one must first identify the relevant erosion regime (vis the extensive study of erosion maps) and also within this regime the material removal mechanism. In simplistic terms, whether oxidation modifies material loss rates due to erosion is a balancing act between ‘how fast the oxide is removed during erosion’ and ‘how quickly the oxide can grow/reform on the erosion damaged surface. If oxide removal rates due to erosion are faster than the growth rate, then the oxide may contribute little to the erosion processes. However, particle impact may have a significant influence on the rate of oxidation, and may also modify the morphology of the oxide formed and also possibly its chemistry.

At the other end of the scale, if the oxidation/corrosion rates are much faster than erosion, then the corrosion processes dominate. In the limit one may find negligible effect of the particle impaction (purely a corrosion/oxidation process), but the erosion particle flux may transport contaminants that lead to higher oxidation rates. The particles may crack the oxide, giving increased short circuit transport, and therefore high corrosion rates, or if sufficiently energetic may lead to chipping of the oxide by classical brittle fracture mechanisms. This thinning of the oxide will lead to faster, albeit still protective, oxidation rates.

Analytical solutions are possible for both of these limiting cases because the underlying material removal mechanisms have been extensively studied – ductile erosion of the metallic substrate or brittle erosion of the oxide scale. Critical questions that need answering in some quantifiable way are;

How does a thin oxide modify the forces transmitted to the substrate and therefore the ductile erosion processes?
When impacting a thick oxide, how thick should it be such that the substrate does not see damage from the particle? Also
When will fracture occur within the oxide rather than propagating to the interface and spalling the complete oxide thickness locally? and how local is 'locally'?

It is this area of substrate/oxide/particle interaction that is impossible to solve analytically, especially as it strongly depends on the particles size and kinetic energy and unfortunately not all particles are the same size. Under these complexed particle/surface interaction conditions the Monte Carlo method offers a solution.

This paper will now concentrate on the Monte Carlo methods required to solve these complexed interaction scenarios that cannot be solved analytically.

Studies of particle/oxide/substrate interactions [35,36] have shown that the degree of surface damage caused by an impact depends on the substrate mechanical properties – a function of temperature, impact dynamics, - scale composition (scale mechanical properties) and scale thickness. Hence, when scales are thin and at sufficiently high temperatures, plastic deformation of the scale is able to accommodate the strains induced by particle impaction. Thus no scale damage results, unless scale is removed when the underlying metallic substrate fails in some ductile way – cutting, ploughing or extrusion.

As the scale thickens, and/or the temperature is reduced, fracture of the oxide can occur. This may be entirely within the oxide – the oxide behaves like a bulk ceramic – but more

likely the cracks will propagate through the oxide down to the metal/oxide interface leading to the loss of oxide by a crack running along this interface (spallation). This will leave areas of non-oxide protected metal and a new scale will grow in the time between impacts, repairing the damage. The new oxide need not be the same as the original oxide; it will depend on the changing substrate composition (due to preferential consumption of some alloying elements), the influence of contaminants transported with the impacting particle and the local gaseous environment. When particle fluxes are high only thin transient scales may form, before further impaction occurs removing both the substrate alloy and any newly formed oxide upon it by one of the prevailing ductile erosion mechanisms.

When the bulk properties of the scale determine the erosion behaviour, scale dominated, using the terminology of Stephenson and Nicholls [47], material removal can be considered in terms of the localised fracture and removal of the scale by “chipping”. Mamoun [67] has modelled this regime analytically by assuming that the difference in kinetic energy at impact and during rebound is a measure of the energy expended in crack growth. From this knowledge of surface cracking he estimates erosion rates.

In developing a Monte Carlo model to predict the complex erosion/oxidation interactions one must identify a parameter which determines whether the oxide is so thin that the system behaves in a ductile manner or so thick that it behaves like a bulk ceramic. Oxide thickness [z] would provide such a measure, but does not account for a variable particle size. The best mnemonic is (z/a) [68] the ratio of the oxide thickness (z) to the radius of the particle impact footprint (a). The latter parameter depends on a combination of particle size, density and velocity.

Thus when z/a is small, less than 0.1 [47], the relative thickness of the oxide is such that the erosion behaviour is controlled by the substrate. When z/a > 0.1 the oxide has a significant influence on the erosion behaviour. Depending on the severity of impact, the oxide may act to protect the substrate – if it does not fracture – or it will spall at the oxide/substrate interface. The way thin ceramic films can protect metal components has been well studied (for example the analysis of Halling and Arnell[69] and this behaviour accounts for the excellent tribological properties of thin ceramic coatings. Whether the oxide fails or not reflects a complex interplay of material properties. Firstly, the stresses as a result of particle impact are the greatest at the metal/oxide interface for thin oxides, but the oxide/metal interface is also most crack resistant. As the oxide thickens the stress at that interface drops, but the formation of less protective oxides, a result of thermal aging, means the interface is more susceptible to crack. Ultimately, the oxide thickens to a stage where the stresses generated at the interface are too low to cause fracture there. This occurs at z/a § 1. If a layered scale is formed cracking and spalling may occur within the scale. Thus erosion proceeds by fracture and removal of discrete volumes of oxide. A brittle erosion mechanism, similar to that observed for ceramic components ensues. The substrate no longer plays a dominant role and we are in an “oxide dominated erosion” region.

Thus using the z/a parameter, one can characterise the different particle/substrate interactions for an oxidised surface. In parallel with these mechanical interactions, the oxide must grow. This is assumed to follow parabolic kinetics, i.e.

$\frac{dz}{dt} = \frac{1}{2z} k_p$ if the scale is still protective or linear kinetics, i.e. $\frac{dz}{dt} = k_l$ if non protective:

The Monté Carlo simulation, developed at Cranfield [63,64] is a two dimensional model. The model allows incremental growth of an oxide on the surface elements, assume a log-normal distribution of impacting particles and calculates material removal rates for each cell in the two dimensional model. The model parameters are those presented in Table 2.

One may ask “How well does the model work?” This strongly depends on the precision of estimates for the material parameters in Table 2. Modern analytical tools (e.g. the nano-indenter) allow measurement of particle, oxide and substrate elastic properties and hardness (from which the yield stress can be estimated), but properties at elevated temperatures are much more difficult to measure. Reliable estimates of oxide fracture stress are available for some oxides, e.g. chromia and alumina[24], but not all. How these change as the surface ages and the oxide grows is unknown. Even with these limitations, this Monté Carlo modelling approach has permitted the prediction of erosion/oxidation rates in this complexed mixed mode erosion/oxidation regime.

As shown in Figure 9, one is able to superimpose erosion rate contours onto erosion/ oxidation maps that take into account the change in erosion/oxidation regime.

Figure 10 illustrates predicted metal loss rates for IN73 8LC impacted at 90°C impact angle, in a particle flux of 0.1 kg/m^2/h at 700°C. At high impact velocities, the erosion rate is dominated by the substrate behaviour. As the impact velocity falls, oxide scales have a chance to form, such that scale removal becomes the controlling mechanism. Under these conditions, the erosion rates drop by a factor of 1000, as a protective oxide glaze is formed.

Figure 11 illustrates a comparison between measured and predicted erosion rates for IN738, aluminised IN738, AT2B coated IN738, AISI 310, and IN800H using the above Monte Carlo model to simulate erosion within a gas turbine under simulated coal fired combined cycle service conditions[63]. The test conditions included impact angles from 15-90°, a variety of erodents, a range of gas velocities from 55-250ms^{-1} and particle loadings between 0.2 and 25 kg/m^2/h at 700°C for exposure times up to 300h. The agreement is very good, within a factor of 3, with predicted erosion rates marginally above those measured, thus providing a conservative estimate of component life.

4. Conclusions

This paper has illustrated the complex nature of the erosion-oxidation process and has covered the numerous factors which affect the system showing that erosion-oxidation is not a trivial issue. Various different mechanisms have been discussed and how the system variables affects the transitions between the different erosion-oxidation regimes. Erosion-oxidation maps play a role by identifying the regime in which a system will be operating and they can help to determine the degree of material wastage that can be expected for a given system. Finally the different concepts of modelling have been discussed showing the versatility of using Monte Carlo statistics in modelling the erosion-corrosion of different systems, giving an accuracy within a factor of 3.

1. I Finnie, *Wear,* 3, (1960) 87.
2. G.P Tilly, *Wear,* 23, (1973) 87.
3. A.V Levy, *Wear,* 108, (1986) 1.
4. C.M Preece, *Conference on the Efects of Crystal Plasticity.*
5. G.P Tilly, *Treatise on Materials Science & Technology,* 13, (1979) 287.
6. B.R Lawn, A.G Evans and D.B Marshall, *Journal of American Ceramic Society* (1980) 574.
7. A.G Evans, M.E Gulden and M Rosenblatt, *Proceedings of the Royal Society* (1978) 343.
8. B Lawn and R Wilshaw, *Journal of Materials Science* , 10, (1975) 1049.
9. C.M Perrott, *Wear,* 45, (1977) 293.
10. S Wada as quoted by S Srinivasan and R.O Scattergood, *Wear,* 128, (1988).
11. S Srinivasan and R.O Scattergood, *Wear,* 128, (1988) 139.
12. I.M Hutchings, *Erosion of Ceramic Materials* (1992) 75.
13. S .M Wiederhorn and B .J Hockey , *Journal of Materials Science and Technology* , 18, (1983) 766.
14. B.R Lawn and M.V Swain, *Journal of Materials Science* , 10, (1975b) 113.
15. B.R Lawn and E.R Fuller, *Journal of Materials Science* , 10, (1975a) 2016.
16. V.D Kristic, *Journal of Materials Science and Technology* , 23, (1988) 259.
17. C.B Ponton and R.D Rawlings, *Materials Science and Technology* , 5, (1989) 865.
18. B.R Lawn and D.B Marshall, *Indentation Fracture & Strength Degradation in Ceramics,* Plenum Press, New York.
19. M Schutze, *Corrosion Science,* 35, (1993) 955.
20. M.M Nagal and W.T Evans, *Journal of Materials Science,* 28, (1993) 6247.
21. P Hancock and J.R Nicholls, *Materials at High Temperature,* 12, (1994) 209.
22. P.Hancock and J.R Nicholls, *Material Science and Technology,* 4, (1988) 398.
23. J.P Wilber, J.R Nichols and M.J Bennet, *The Institute of Materials London,* 1997.
24. D.J Stephenson and J.R Nicholls, *Wear,* 186-187, (1995) 284.
25. W Tabakoff, *Surface and Coatings Technology,* 120-12 1, (1999) 542.
26. P.M Rogers, I.M Hutchings and J.A Little, *Wear,* 186-187, (1995) 238.
27. P.M Rogers, T.E Howes, I.M Hutchings and J.A Little, *Wear,* 186-187, (1995) 306.
28. T.E Howes, P.M Rogers, I.M Hutchings and J.A Little, *Wear,* 186-187, (1995) 316.
29. V.K Sethi and R.G Corey, *Proceedings of the 7th International Conference on Erosion by Liquid and Solid Impact,* 1987.
30. S Chinnadurai and S Bahadur, *Wear,* 186-187, (1995) 299.
31. P Hancock, J.R Nicholls and D.J Stephenson, *Surface and Coatings Technology,* 32, (1987) 285.
32. A Levy and Y.F Man, *Wear,* 111 , (1986) 173.
33. A Levy, J Yan and J Paterson, *Wear,* 108, (1986) 43.
34. N Gat and W Tabakoff, *Wear,* 50, (1978) 85.
35. D.J Stephenson, J.R Nicholls and P Hancock, *Wear,* 111, (1986) 15.
36. D.J Stephenson, J.R Nicholls and P Hancock, *Wear* (1986) 31.
37. M Suckling and C Allen, *Wear,* 203-204, (1997) 528.
38. M.M Stack and D Pena, *Surface and Coatings Technology,* 113, (1999) 5.
39. M.M Stack, Q Song-Roehrle, F.H Stott and G.C Wood, *Wear,* 181-183, (1995) 516.
40. M.M Stack, J Chacon-Nava and F.H Stott, *Wear,* 180, (1995) 91.
41. R.L Howard and A.Ball, *Wear,* 205 , (1997) 11.
42. J.R Zhou and S Bahadur, *Wear,* 181-183, (1995) 178.
43. A.L Ham, J.A Yeomans and J.F Watts, *Wear,* 233-235, (1999) 237.
44. J.R Nicholls, *Corrosion in Advanced Power Plants, Proc. 2n Int. Workshop on Corrosion in Advanced Power Plants, Tampa , Florida (* 1997) 219.
45. I.G Wright, *Corrosion in Advanced Power Plants, Proc. 2n Int. Workshop on Corrosion in Advanced Power Plants, Tampa , Florida (* 1997) 207.
46. I.G Wright, V.K Sethi and J Stringer, *Proc. 2nd Int Conf. on Heat Resistant Materials, Tennessee,* 1995.

47. D.J Stephenson and J.R Nicholls, *Corrosion Science,* 35, (1993) 1015.
48. A.J Markworth, *Materials Science and Engineering A,* A150, (1992) 37.
49. A.J Markworth, V Nagarajan and I.G Wright, *Oxidation of Metals,* 35, (1991) 89.
50. M.M Stack and F.H Stott, *Corrosion Science,* 35, (1993) 1027.
51. M.M Stack and D Pena, *Wear,* 251, (2001) 1433.
52. M.M Stack, *Corrosion in Advanced Power Plants, Proc. 2n Int. Workshop on Corrosion in Advanced Power Plants, Tampa , Florida (* 1997) 243.
53. S Hogmark, A Hammarsten and S Soderberg, *Proc. 6th Int. Conf. On Erosion by Solid and Liquid Impact* (1983) 37.
54. R.H Barkalow and F.S Pettit, *Corrosion/Erosion of Coal Conversion System Materials, Berkley USA,* 1979.
55. M Roy, K.K Ray and G Sundararajan, *Metallurgical and Materials Transactions A,* 32A, (2001) 1431.
56. D.J Stephenson and J.R Nicholls, *Wear,* 186-187, (1995) 284.
57. C.T Kang, F.S Pettit and N Birks, *Metallurgical Transactions* , A 18, (1987) 1785.
58. I.G Wright, V.K Sethi and A.J Markworth, *Wear,* 186-187, (1995) 230.
59. D.M Rishel, F.S Pettit and N Birks, *Corrosion Science,* 35, (1993) 1007.
60. G.J Holtzer and P.L.F Rademakers, E.J Anthony , *11th Int Conf on Fluidized Bed Combustion,* ASME, New York, 1991.
61. A.V Levy and Y.F Man, *Wear,* 131, (1989) 39.
62. Q Geng, B Wang, P Hou and A.V Levy, *Wear,* 150, (1991) 89.
63. J.R Nicholls and D.J Stephenson, *Wear,* 186-187, (1995) 64.
64. D.J Stephenson and J.R Nicholls, *Plant Corrosion - Prediction of Materials Performance,* Ellis Horwood LtD, 1987.
65. R.G Wellman and J.R Nicholls, *Euromat 2001, Rimini Italy,* 2001.
66. R.G Wellman, *Ph.D. Thesis, Cranfield University* (2001).
67. M Mamoun, *Argonne National Laboratory Report, ANL-75-XX-2* (1975).
68. D.J Stephenson and J.R Nicholls, *Materials Science and Technology,* 6, (1990) 96.
69. J Halling and R. D Arnell, *Wear,* 100, (1984) 367.

M Roy [55]	Metal Erosion	Oxidation affected erosion	Oxidation controlled erosion	Oxide erosion
D.J Stephenson [56]	Substrate dominated	Oxide modified	Oxide dominated	Oxidation kinetics
R. H Barklow [54]	Metallic erosion	Oxidation modified erosion	Erosion modified oxidation	Oxidation
C.T Kang [57]	Pure erosion	Oxidation affected erosion	Erosion enhanced oxidation	erosion of oxide only
M.M Stack [50]	Erosion dominated	Erosion corrosion dominated	Corrosion dominated 1	Corrosion dominated 2
I.G Wright et al [58]	Erosion dominates	Erosion oxidation interaction		Oxidation dominates

a)

S Hogmark [53]	Pure erosion	Erosion of oxide and substrate	Flaking of oxide at each impact	Erosion of oxide without flaking	Erosion affected corrosion	Pure oxidation
D. M Rishell [59]	Pure erosion	Oxidation affected erosion	Intermittent spalation after thickness reached	Thicker oxide by induced defects changing kinetics	Thinning of oxide by erosion, change in kinetics giving steady state process.	Oxidation

b)

Table 1: Table of various proposed erosion-oxidation regimes (divided in a) 4step and b) 6 step processes).

Particle properties	Particle loading Mean particle size Standard deviation in particle size Density Elastic modulus Poisson's ratio Shape factor
Alloy Properties	Density Elastic modulus Poisson's ratio Yield stress Failure strain Work hardening exponent
Surface Scale Properties	Density Elastic Modulus Poisson's ratio Thickness/rate constant Fracture stress
Environmental Properties	Temperature Exposure time Gas/particle velocity

Table 2: Input parameters needed for Monte Carlo erosion modelling [47].

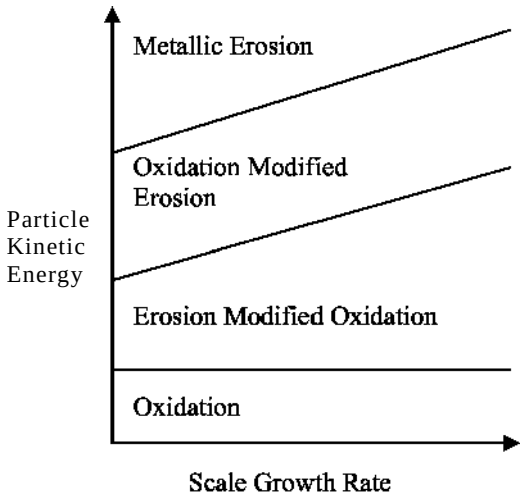

Figure 1: Schematic diagram of how oxidation kinetics and particle impact energy influence E-O wastage [54].

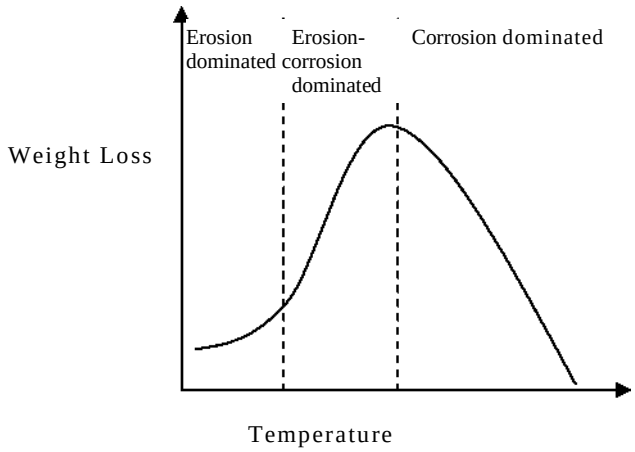

Figure 2: Diagram showing the erosion-corrosion response of metals to temperature changes [40].

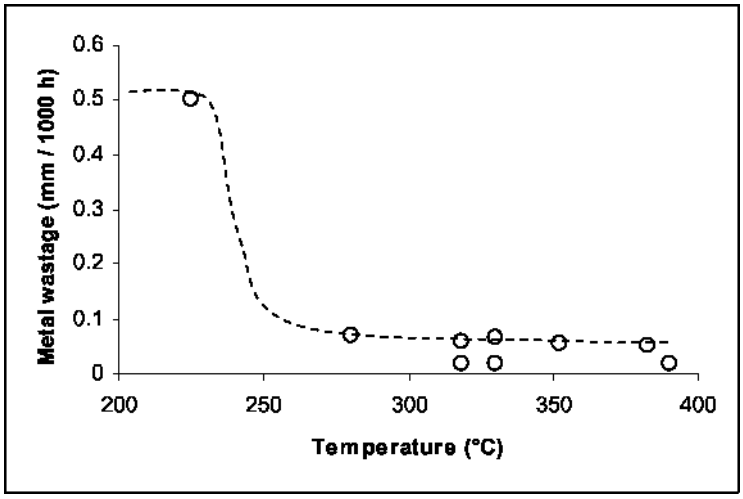

Figure 3: Effect of temperature on material wastage rates in FBC's for plain carbon steel in the 4 MWth AFBC at TNO Apeldoorn, The Netherlands, bed temperature 850°C re-plotted from Holtzer and Rademakers [60].

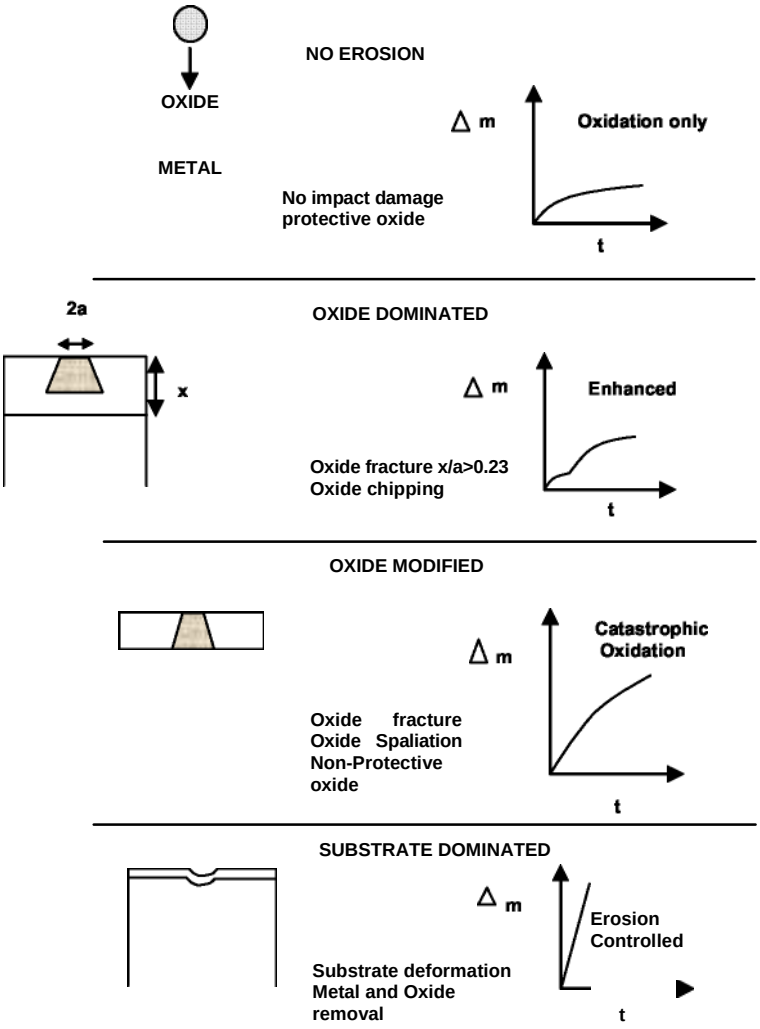

Figure 4: Schematic of the different erosion-oxidation regimes proposed by Stephenson and Nicholls [56].

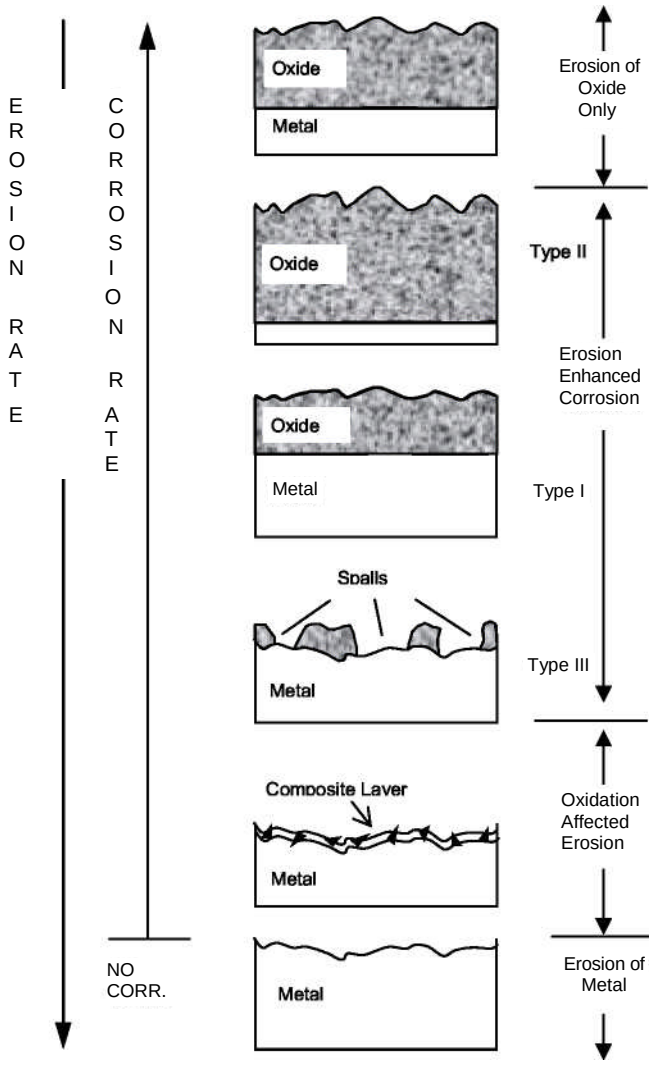

Figure 5: Schematic of the different erosion-oxidation regimes proposed by Rishel et al[59].

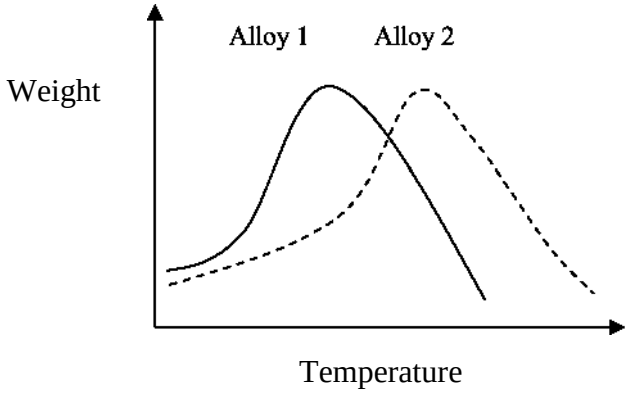

Figure 6: Schematic showing how alloy content can affect the erosion-corrosion rate with temperature increases (corrosion rate of Alloy 1 > Alloy2) [40].

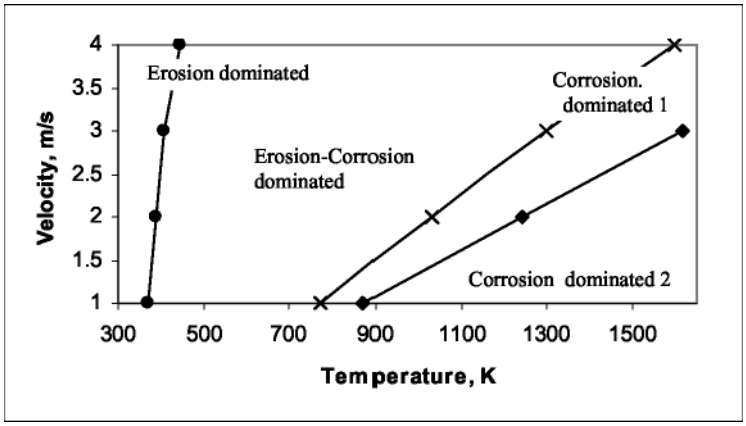

Figure 7: E-O map evaluated by Stack's simulation program [50].

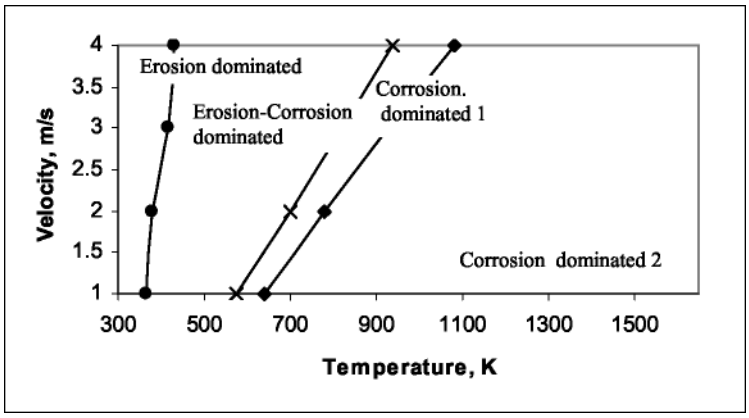

Figure 8: E-O map showing how boundaries change if the oxidation rate is increased by 10^2 [50].

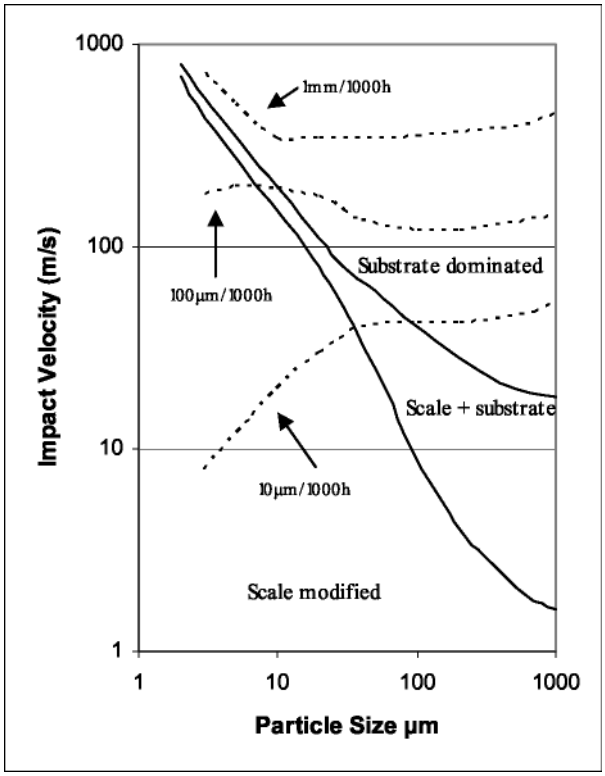

Figure 9: E-O map for IN 738 impacted at 90° by silica beads at 700°C [24].

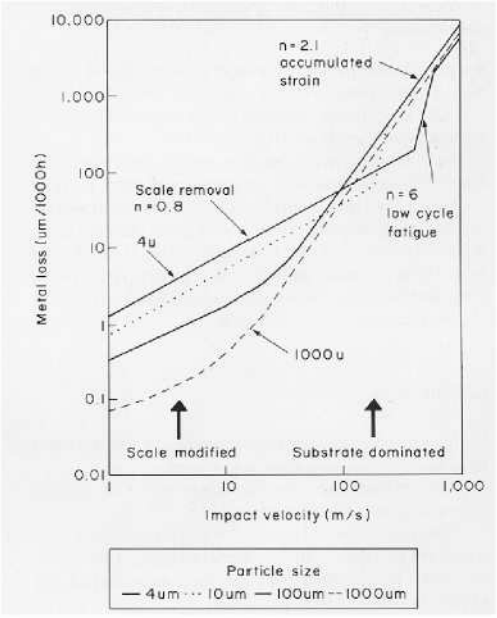

Figure 10: Predicted metal loss rates for IN738LC impacted at 90°C impact angle, in a particle flux of 0.1 kg/m^2/h at 700°C [63].

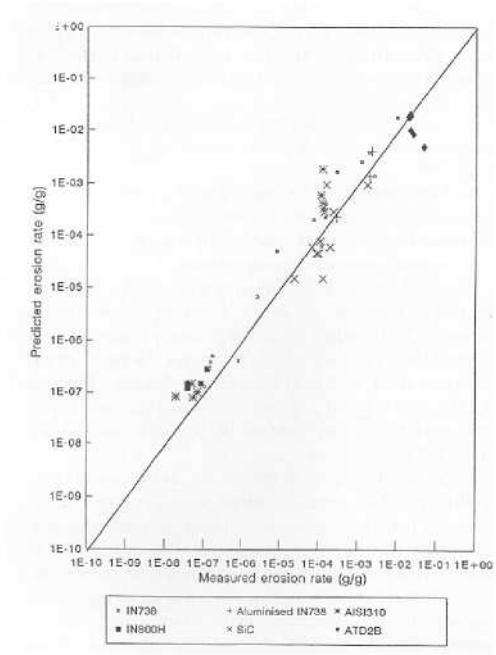

Figure 11: Graph of measured and predicted erosion rates for different materials [63].

High Temperature Erosion-Oxidation Mechanisms, Maps and Models

Wellman, R. G.

2004-05-01T00:00:00Z

R. G. Wellman and J. R. Nicholls, High temperature erosion-oxidation mechanisms, maps and models, Wear, Volume 256, Issues 9-10, May 2004, Pages 907-917.
http://dx.doi.org/10.1016/j.wear.2003.04.003